Cholinergic and glutamatergic agonists induce gamma frequency activity in dorsal subcoeruleus nucleus neurons

Christen Simon, Nebojsa Kezunovic, D. Keith Williams, Francisco J. Urbano and E. Garcia-Rill

Am J Physiol Cell Physiol 301:C327-C335, 2011. First published 4 May 2011;
doi:10.1152/ajpcell.00093.2011

Am J Physiol Cell Physiol 301: C327–C335, 2011.
First published May 4, 2011; doi:10.1152/ajpcell.00093.2011.

Cholinergic and glutamatergic agonists induce gamma frequency activity in dorsal subcoeruleus nucleus neurons

Christen Simon,[1] Nebojsa Kezunovic,[1] D. Keith Williams,[2] Francisco J. Urbano,[3] and E. Garcia-Rill[1]

Center for Translational Neuroscience, Departments of Neurobiology and [1]Developmental Sciences, [2]Biometry, University of Arkansas for Medical Sciences, Little Rock, Arkansas; and Instituto de Fisiologia, Biologia Molecular, y [3]Neurociencias IFIBYNE-CONICET, University of Buenos Aires, Buenos Aires, Argentina

Submitted 30 March 2011; accepted in final form 29 April 2011

Simon C, Kezunovic N, Williams DK, Urbano FJ, Garcia-Rill E. Cholinergic and glutamatergic agonists induce gamma frequency activity in dorsal subcoeruleus nucleus neurons. *Am J Physiol Cell Physiol* 301: C327–C335, 2011. First published May 4, 2011; doi:10.1152/ajpcell.00093.2011.—The dorsal subcoeruleus nucleus (SubCD) is involved in generating two signs of rapid eye movement (REM) sleep: muscle atonia and ponto-geniculo-occipital (PGO) waves. We tested the hypothesis that single cell and/or population responses of SubCD neurons are capable of generating gamma frequency activity in response to intracellular stimulation or receptor agonist activation. Whole cell patch clamp recordings (immersion chamber) and population responses (interface chamber) were conducted on 9- to 20-day-old rat brain stem slices. All SubCD neurons ($n = 103$) fired at gamma frequency when subjected to depolarizing steps. Two statistically distinct populations of neurons were observed, which were distinguished by their high (>80 Hz, $n = 24$) versus low (35–80 Hz, $n = 16$) initial firing frequencies. Both cell types exhibited subthreshold oscillations in the gamma range ($n = 43$), which may underlie the gamma band firing properties of these neurons. The subthreshold oscillations were blocked by the sodium channel blockers tetrodotoxin (TTX, $n = 21$) extracellularly and *N*-(2,6-dimethylphenylcarbamoylmethyl)triethylammonium bromide (QX-314) intracellularly ($n = 5$), indicating they were sodium channel dependent. Gamma frequency subthreshold oscillations were observed in response to the nonspecific cholinergic receptor agonist carbachol (CAR, $n = 11$, $d = 1.08$) and the glutamate receptor agonists *N*-methyl-D-aspartic acid (NMDA, $n = 12$, $d = 1.09$) and kainic acid (KA, $n = 13$, $d = 0.96$), indicating that cholinergic and glutamatergic inputs may be involved in the activation of these subthreshold currents. Gamma band activity also was observed in population responses following application of CAR ($n = 4$, $P < 0.05$), NMDA ($n = 4$, $P < 0.05$) and KA ($n = 4$, $P < 0.05$). Voltage-sensitive, sodium channel-dependent gamma band activity appears to be a part of the intrinsic membrane properties of SubCD neurons.

arousal; carbachol; kainic acid; *N*-methyl-D-aspartic acid; rapid eye movement sleep

DURING THE ACTIVATED STATES of waking and rapid eye movement (REM) sleep, EEG responses are characterized by low-amplitude, high-frequency neuronal activity in the gamma range (≈20–80 Hz). Gamma frequency oscillations have been proposed to participate in sensory perception, problem solving, memory, and REM sleep (15, 17, 30, 31, 41), and it has been suggested that such coherent events occur at cortical or thalamocortical levels (23, 35). The mechanism behind such activity in the cortex includes intrinsic, sodium-dependent subthreshold oscillations (23), which underlie the firing of action potentials (AP). Gamma oscillations also have been recorded in the hippocampus (43) and cerebellum (27).

Nuclei located in the pons, including the dorsal subcoeruleus nucleus (SubCD), are critical for generation of REM sleep (3, 5, 6, 12, 25, 29, 44). Lesion of this area produced REM sleep without muscle atonia or ponto-geniculo-occipital (PGO) waves (21, 26, 29, 33), or diminished REM sleep (24). The SubCD is most active during REM sleep (5, 13), and injection of the nonspecific acetylcholine receptor agonist carbachol (CAR) or the glutamatergic receptor agonist kainic acid (KA) into this area induced a REM sleep-like state with muscle atonia (2, 28, 38, 44). The SubCD receives afferents from several nuclei, including the pedunculopontine nucleus (PPN) (11). Sodium-dependent subthreshold oscillations have been discovered in some PPN neurons, but the maximum frequency of activity was 30 Hz (36). Recent results from our lab described the presence of gamma band activity in the PPN, a mechanism due to the presence of P/Q-type voltage-gated calcium channels (22). Subthreshold oscillations have yet to be described in the SubCD.

Extracellular recording studies in the SubCD in the cat reported tonic firing in the gamma range during REM sleep (9). In vitro SubC neurons fired at gamma frequency in response to depolarizing current steps, although a firing rate plateau was not determined and, the study included cholinergic and tyrosine hydroxylase-positive neurons outside of the SubCD (6). In contrast, the SubCD has been reported to contain only glutamatergic neurons (7) and perhaps GABAergic neurons. In the present study, we examined maximal AP frequencies of SubCD neurons, investigated intrinsic properties underlying subthreshold oscillations, and determined how cholinergic and glutamatergic inputs modulate their gamma band activation.

Considering the role of the SubCD in generating REM sleep, we suggest that this nucleus can promote gamma band activity. However, does the SubCD simply trigger gamma activity in its targets, or does the SubCD have the intrinsic properties necessary for generating its own gamma band activity and driving its targets with this activity? We tested the hypothesis that SubCD neurons exhibit gamma band activity in terms of AP frequency and subthreshold oscillations in single cells, and the population as a whole generates gamma band activity when pharmacologically activated.

METHODS

All experimental protocols were approved by the Institutional Animal Care and Use Committee of the University of Arkansas for Medical Sciences and were in agreement with the National Institutes of Health guidelines for the care and use of laboratory animals.

Address for reprint requests and other correspondence: E. Garcia-Rill, Center for Translational Neuroscience, Dept. of Neurobiology and Developmental Sciences, Univ. of Arkansas for Medical Sciences, Slot 847, 4301 West Markham St., Little Rock, AR 72205 (e-mail: GarciaRillEdgar@uams.edu).

Slice preparation. Pups aged 9–20 days from adult timed-pregnant Sprague-Dawley rats (280–350 g) were anesthetized with ketamine (70 mg/kg im) until tail pinch reflex was absent. This age range was selected because it spans the developmental decrease in REM sleep of the rat that occurs between 10 and 30 days (20). Pups were decapitated and the brain was rapidly removed and cooled in oxygenated sucrose-artificial cerebrospinal fluid (sucrose-aCSF). The sucrose-aCSF consisted of (in mM) 233.7 sucrose, 26 $NaHCO_3$, 3 KCl, 8 $MgCl_2$, 0.5 $CaCl_2$, 20 glucose, and 0.4 ascorbic acid. Sagittal sections (400 μm) containing the SubCD were cut and slices were allowed to equilibrate in aCSF at room temperature for 1 h. The aCSF was composed of (in mM) 117 NaCl, 4.7 KCl, 1.2 $MgSO_4$, 2.5 $CaCl_2$, 1.2 NaH_2PO_4, 24.9 $NaHCO_3$, and 11.5 glucose. Some experiments were performed using low Mg^{2+} aCSF with the following composition (in mM): 117 NaCl, 4.7 KCl, 2.5 $CaCl_2$, 1.2 NaH_2PO_4, 20 glucose, and 24.9 $NaHCO_3$.

Whole cell patch clamp recordings. Slices were recorded at 37 ± 2°C while perfused (1.5 ml/min) with oxygenated (95% O_2-5% CO_2) aCSF in an immersion chamber. Differential interference contrast optics was used to visualize neurons using an upright microscope (Nikon FN-1, Nikon). Recordings were performed using borosilicate glass capillaries pulled using a P-97 puller (Sutter Instrument, Novato, CA) and filled with a solution of (in mM) 124 K-gluconate, 10 HEPES, 10 phosphocreatine di-tris, 0.2 EGTA, 4 Mg_2ATP, and 0.3 Na_2GTP. In some studies, the intracellular sodium channel blocker *N*-(2,6-dimethylphenylcarbamoylmethyl)triethylammonium bromide (QX-314, 5 mM) was added. Osmolarity was adjusted to ~270–290 mosM and pH to 7.4. The pipette resistance was 3–5 MΩ, the liquid-junction potential was ~9 mV for pipettes filled with K-gluconate intracellular solution, and the reported voltages were not corrected for this value. Only cells with a stable, resting membrane potential of −48 mV or more negative and with access resistance <20 MΩ were used. No series resistance compensation was performed in this study. All recordings were made using a Multiclamp 700B amplifier (Molecular Devices, Sunnyvale, CA) in current clamp mode. Analog signals were low-pass filtered at 2 kHz and digitized at 5 kHz using a Digidata-1440A and pClamp10 software (Molecular Devices).

When needed, current (0 to −50 pA) was injected to maintain the membrane potential of the recorded cells at −60 mV. The following intrinsic membrane properties were characterized: resting membrane potential, AP threshold (determined by the first AP that appeared in current-voltage steps), AP amplitude, AP halfwidth duration, input resistance (R_{in}), and membrane time constant (τ, determined by fitting a single exponential decay function to the initial 25–100 ms of a −40 pA hyperpolarizing current step). We also analyzed the responses to depolarizing steps (500 ms duration, 2.5-s interpulse interval) in current clamp mode to determine the maximal or close to maximal firing frequencies of SubCD neurons. Subthreshold oscillations were measured in current clamp mode at membrane potentials between −48 and −35 mV, and, when the membrane potential was above AP threshold, subthreshold oscillations were measured between APs.

Population response recordings. For population studies, we used a BSC-1 interface chamber (Automate, Berkeley, CA), and the slice was visualized with a Wild dissection microscope. Recordings were made with borosilicate glass capillaries pulled to a 1- to 2-μm tip with 1–2 MΩ resistance and filled with aCSF. Recordings were amplified with a Grass Instrument (Quincy, MA) P511 amplifier, bandpass filtered at 1 Hz-1 kHz, and digitized with a Digidata-1332A at a rate of 10 kHz.

Drug application. Drugs were administered to the slice via a peristaltic pump (Cole-Parmer, Vernon Hills, IL) and a three-way valve system, such that solutions reached the slice 1.5 min after the start of application. To test the ionic mechanism of subthreshold oscillations, the intracellular QX-314 (5 mM), and extracellular tetrodotoxin citrate (TTX, 0.01–10 μM) sodium channel blockers were used. The effects of the nonspecific cholinergic agonist CAR (10–50 μM) and glutamatergic receptor agonists KA (0.2–10 μM) and *N*-methyl-D-aspartic acid (NMDA 1–10 μM) were also tested. When measuring subthreshold oscillations, fast excitatory and inhibitory synaptic transmission was blocked using the selective NMDA receptor antagonist 2-amino-5-phosphonovaleric acid (APV 40 μM), the KA receptor antagonist 6-cyano-7-nitroquinoxaline-2,3-dione (CNQX 10 μM), the $GABA_A$ receptor antagonist gabazine (GBZ 10 μM), and the glycine receptor antagonist strychnine (STR 10 μM). All drugs were purchased from Sigma (St. Louis, MO), except TTX, which was purchased from Tocris Bioscience (Ellisville, MO). When the responses of SubCD neurons to NMDA was recorded, a Mg^{2+} free aCSF was used to relieve the Mg^{2+} block of this receptor.

Data analysis. Off-line analyses were performed using Clampfit software (Molecular Devices, Sunnyvale, CA). The interspike interval (ISI) was measured to determine the maximal or close to maximal firing frequency during the beginning, middle, and end of depolarizing current steps. In addition, continuous measurement of instantaneous firing frequency was carried out. Recordings of membrane oscillations were bandpass filtered (8-pole Bessel with 20 Hz cutoff high-pass filter and 8-pole Chebyshev 59 Hz cutoff low-pass filter), followed by power spectrum analysis using pClamp10 software to quantify gamma band frequency activity. Further analysis was conducted using MatLab software (The MathWorks, Natick, MA). Plots of the event-related spectral perturbation (ERSP) for each population response were generated with the EEGLAB MatLab Toolbox (14), as has been described previously (34).

To determine the effect size of agonists on single neurons, standardized mean difference was used to calculate the Cohen's *d* value. A value >0.8 was considered to indicate a large difference between control and agonist exposure. Analysis conditions for population responses consisted of 20-s windows every 1 min before drug application, during the peak effect, and after the agent had been washed out of the bath. These analyses generated power spectra for a particular point in time. Amplitudes of power spectra for each group of four slices were tabulated at 0–55 Hz, and a mean of the amplitudes at each frequency was calculated for each group of slices, e.g., control, neuroactive agent, and wash. A repeated-measures ANOVA model was fit for each response using SAS Proc Mixed software (SAS Institute, Cary, NC). Because different concentrations and frequencies were determined in each group of slices, a covariance structure existed for measurements within groups of slices. Concentration, frequency, and concentration-by-frequency standard errors (SE) were estimated using White's empirical covariance structure estimation method. If concentration-by-frequency interaction terms for a specific response were significant at the 5% level, the focus of the differences among concentration levels was assessed according to specific levels of frequency. The Tukey approach was employed to control for multiple comparisons. *F* values and degrees of freedom were reported for all linear regression ANOVAs. Differences were considered significant at values of $P \leq 0.05$. All results are presented as means ± SE.

RESULTS

Whole cell patch clamp recordings were performed in a total of $n = 103$ SubCD neurons, localized as previously described (18, 19). All neurons were located within a region ~500 μm in diameter anterior to the seventh nerve. Although tyrosine hydroxylase immunocytochemistry was not performed, all recordings were well ventral to the locus coeruleus. Previous studies found no cholinergic cells in this region (19). We did not attempt to identify different morphological or neurotransmitter types in this population but suspect they represent a mixture of glutamatergic and GABAergic neurons. As our results demonstrate, all cells types in SubCD had similar properties.

Firing properties of SubCD neurons. Maximal firing frequency was determined in $n = 40$ of the recorded neurons, using steps of increasing current amplitudes in current clamp

mode. This protocol applied nine 500-ms duration current steps with an increase of 30 pA for each step and 2.5-s interstep interval. The final current step was 270 pA greater than the current injection required to hold the cell at −60 mV. During the current steps, the cells were depolarized and fired APs when above threshold, usually reaching a steady membrane potential of −20 mV. Firing frequency was determined by measuring the ISI between the first two, middle two (determined by measuring the ISI between the two APs 250 ms following the beginning of the step), and final two APs during each current step. In addition, continuous measurement of instantaneous firing frequency was carried out.

The initial ISI of each neuron was measured during the highest amplitude (270 pA) current step and converted to frequency (Fig. 1*A*). Cells were divided into two cell types distinguished by their high (>80 Hz, circles, $n = 24$) versus low (35–80 Hz, squares, $n = 16$) initial AP frequency during the beginning of the 270-pA current step. Records of the responses for both cell types were truncated and spliced together to show only three of the current steps, including the 270-pA step (dashed line, Fig. 1*B*). A higher resolution view of the 270-pA step shows instantaneous changes in AP frequency.

A graph of AP frequency during the beginning (closed circle), middle (closed triangle), and end (closed inverted triangle) of each current step was generated for the high (*left*) and low (*right*) frequency cell types (Fig. 1*C*). The AP frequency of both cell types increased with greater amplitude current steps. The high frequency cell type fired APs at >80 Hz at the beginning of the 270-pA current step, with mean of 152 ± 19 Hz. In contrast, measuring AP frequency during the middle and end of the 270-pA current step revealed a slowing of AP frequency to gamma frequencies (middle, 53 ± 5 Hz; end, 42 ± 4 Hz). The slow frequency cell type fired at gamma frequencies at the beginning (55 ± 3 Hz), middle (51 ± 2 Hz),

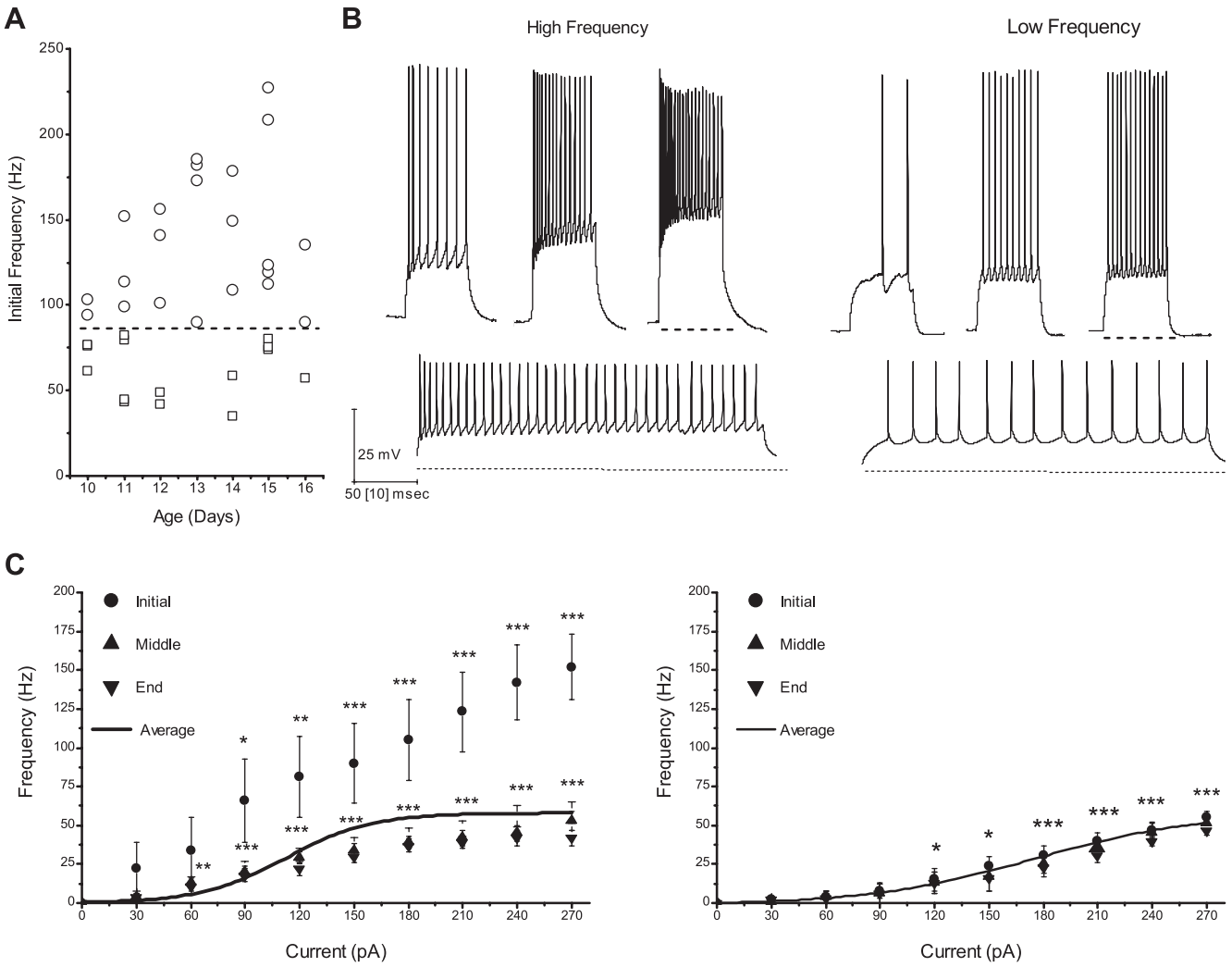

Fig. 1. Gamma band activity in whole cell recorded dorsal subcoeruleus nucleus (SubCD) neurons. *A*: maximal action potential (AP) frequency was measured using current steps (each step was 500 ms in duration with an increase of 30 pA per step and a 2.5-s latency between steps). Cells were divided into two cells types distinguished by their initial AP frequency during the highest amplitude current step (270 pA). The first type (circles) fired at high frequency (>80 Hz), whereas the second type (squares) fired at lower frequency (35–80 Hz) during the initiation of the response. *B*: records were truncated and spliced together to show only three current steps for both the high (*left*) and low (*right*) frequency cell types. The 270 pA current step is underlined and expanded in the lower records to show instantaneous changes in AP frequency. *C*: average of the first, middle, and end intersike intervals (ISIs) (converted to frequency) of the neurons classified in the high (*left*) and the low (*right*) frequency cell types. The black line shows the average instantaneous firing frequency during the entire current step (***$P < 0.001$, **$P < 0.01$, *$P < 0.05$ compared with baseline).

and end (47 ± 2 Hz) of the 270-pA current step (Fig. 1*C*, *right*). A one-way ANOVA was performed to compare the AP frequencies at the beginning, middle, and end of the 270-pA current step between the high and low frequency cell types. The high frequency cell type was found to have a significantly greater initial AP frequency compared with the AP frequency during the middle and end of the current step, as well compared with the beginning, middle, and end of the slow frequency cell type [$F = 60.12$ (5, 114), $P < 0.001$].

There appears to be two cell types in the SubCD that are distinguished by their initial firing frequencies following a stimulus. The AP frequency of both cell types increased with greater amplitude current steps. However, the AP frequency of the high frequency cell type decreased during each step, while the firing rate of the slow frequency cell type remained constant during the entire current step. The AP frequency of both cell types settled in the gamma range.

Next, the properties of these two cell types were analyzed (Table 1). This table includes the neurons ($n = 40$) that were incorporated into Fig. 1. There was no significant difference in R_{in} between the two cell types [two sample *t*-test, $t = 0.56$, $df = 20$, $P > 0.05$], suggesting that the initial increase in firing frequency observed in the high frequency cell type was not due to a difference in R_{in}. The only difference between the cell types was the presence of low-threshold spike (LTS) currents in over one-half of the high-frequency cells, with no low frequency cells exhibiting LTSs.

Voltage-dependent subthreshold oscillations in SubCD neurons. We tested the possibility that subthreshold oscillations might underlie the gamma frequency firing properties of SubCD neurons ($n = 43$). Inhibitory and excitatory spontaneous synaptic activity was blocked with APV, CNQX, GBZ, and STR to isolate subthreshold oscillations. At membrane potentials below AP threshold (Fig. 2*A*, −48 mV), subthreshold oscillations were observed and persisted at membrane potentials above AP threshold, where they were evident between APs (Fig. 2*A*, −43 mV). Subthreshold oscillations were also observed following inactivation of sodium channels underlying APs (Fig. 2*A*, −40 mV), suggesting the existence of two populations of voltage-gated sodium channels: one related to AP generation and the other related to subthreshold oscillations. The oscillation amplitude appeared to increase at less negative membrane potentials, but the variability was very large, making it difficult to measure oscillation amplitude (see records, Fig. 2*A*). A power spectrum revealed the presence of subthreshold oscillations in the gamma frequency range (Fig. 2*B*).

Table 1. *Properties of SubC neurons according to response to depolarizing steps*

Property	High Frequency ($n = 24$)	Low Frequency ($n = 16$)
Low threshold spikes	$n = 13$ (54.17%)	$n = 0$
Resting membrane potential, mV	−51.92 ± 2.56	−53.23 ± 1.85
Input resistance, MΩ	565.54 ± 71.69	473.75 ± 77.29
Time constant, ms	24.27 ± 1.88	25.01 ± 2.80
Action potential threshold, mV	−39.63 ± 0.76	−37.56 ± 2.32
Action potential amplitude, mV	59.45 ± 2.36	59.50 ± 1.99
Action potential half-width, ms	0.98 ± 0.07	1.11 ± 1.98

Values are means ± SE; n = number of cells. SubCD, dorsal subcoeruleus nucleus.

TTX ($n = 21$) was superfused to determine the pharmacological profile of sodium channels underlying gamma oscillations. Low concentration of TTX (0.01 μM, Fig. 2*C*) completely blocked AP generation and reduced the power of gamma band oscillations, whereas high concentration of TTX (10 μM, Fig. 2*C*) completely blocked the remaining subthreshold gamma oscillations. A sodium-dependent mechanism was further confirmed using QX-314 ($n = 5$) in the intracellular solution, which blocked both APs and subthreshold gamma oscillations (Fig. 2*D*). Power spectra of the oscillations before and after TTX (Fig. 2*E*, *left*) or QX-314 (*right*) further confirmed the subthreshold oscillations were blocked. These gamma frequency, sodium-dependent subthreshold oscillations may underlie the gamma frequency AP firing of SubCD neurons observed in Fig. 1.

Subthreshold oscillations were observed at holding potentials greater than the resting membrane potential of the neuron (Fig. 2). Summation of excitatory inputs, such as glutamate and acetylcholine, might provide the membrane depolarization necessary for generation of gamma frequency oscillations and APs. Therefore, we recorded SubCD neurons before and after bath application of NMDA ($n = 12$), KA ($n = 13$), or CAR ($n = 11$) (Fig. 3). NMDA (Fig. 3*A*) induced a depolarization of the membrane potential sufficient to generate subthreshold gamma oscillations between APs. A power spectrum of the oscillations revealed a high amplitude peak at 28 Hz (*right*, $d = 1.09$). Subthreshold oscillations were also observed following KA superfusion (Fig. 3*B*, $d = 0.96$), which exhibited a high amplitude peak in the power spectrum at 21 Hz (*right*). Gamma frequency subthreshold oscillations were also observed after CAR application (Fig. 3*C*), with gamma peaks in the power spectrum at 23 and 34 Hz (*right*, $d = 1.08$). Excitatory inputs to the SubCD appear to provide the necessary excitation for the generation of gamma frequency subthreshold oscillations.

Population response recordings. In the foregoing experiments (Figs. 1–3), we discovered that gamma band activity may be an intrinsic property of SubCD neurons that can be activated by membrane potential depolarization mediated by cholinergic and glutamatergic agonists. For the SubCD to activate its efferent targets at gamma frequency, the whole population of neurons would be required to be active at gamma frequencies. Therefore, we tested whether gamma band activity can also be generated by the population of neurons in the SubCD in response to glutamatergic or cholinergic inputs, using population response recordings.

Population responses were recorded following NMDA exposure ($n = 4$, Fig. 4*A*). The power spectrum of the recordings revealed an overall increase in activity as well as specific peaks in the alpha and gamma ranges for the population as a whole (Fig. 4*B*). One-way repeated measures ANOVA revealed a statistically significant increase in activity following NMDA administration [$F = 115.37$ (2, 6), $P < 0.001$], with peaks at 10 Hz ($P < 0.001$), 15 Hz ($P < 0.01$), 25 Hz ($P < 0.001$), 30 Hz ($P < 0.01$), 35 Hz ($P < 0.001$), 40 Hz ($P < 0.05$), 45 Hz ($P < 0.001$), 50 Hz ($P < 0.01$), and 55 Hz ($P < 0.001$). A graph of ERSP was generated using 9 min of recordings during NMDA exposure and 2 min following exposure/during washout (Fig. 4*C*). NMDA took effect at *minute 3* and the peak effect was observed between *minutes 5* and *9*, when NMDA induced specific peaks of activity in the alpha, low gamma, and mid

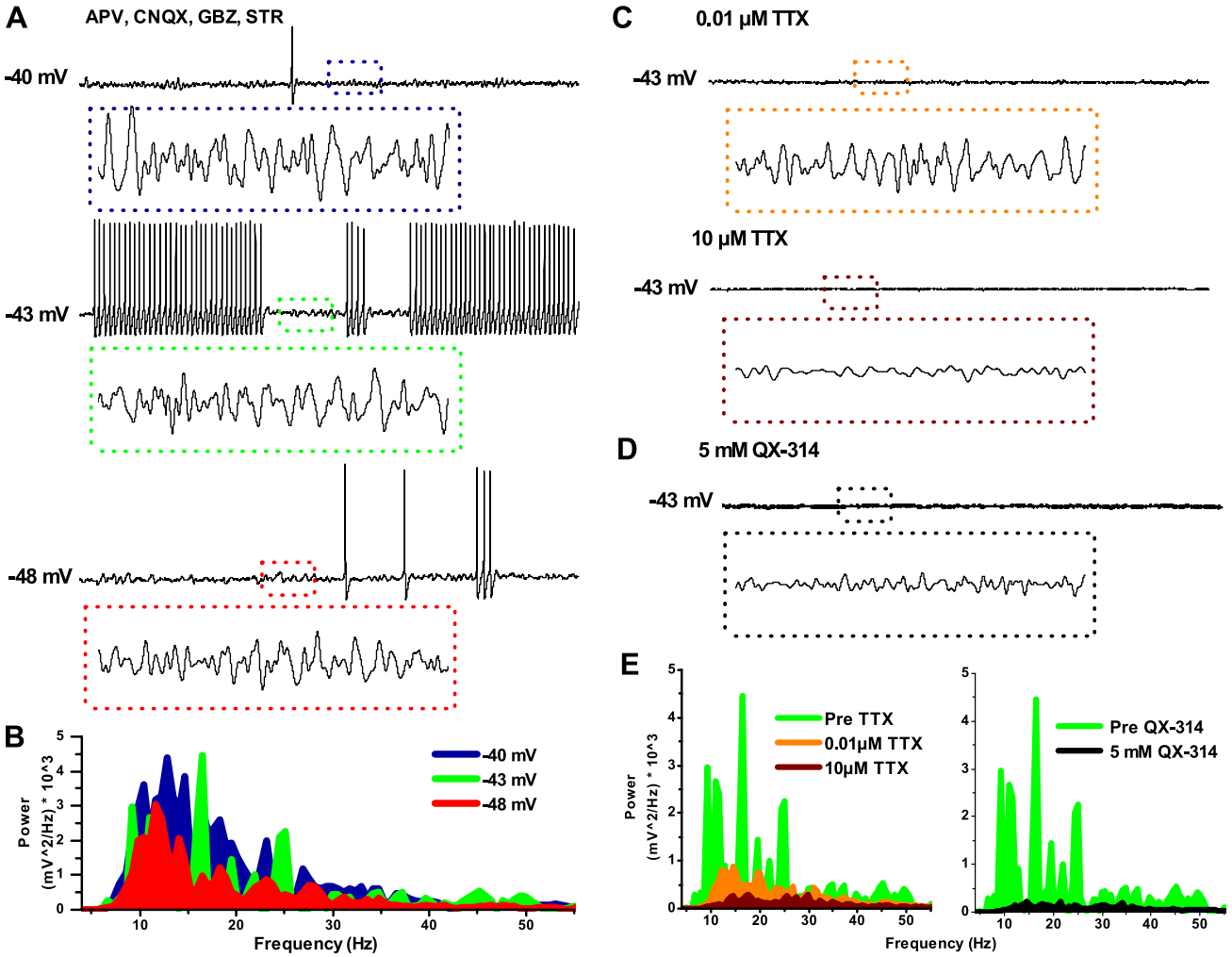

Fig. 2. Sodium-dependent subthreshold oscillations in SubCD neurons. *A*: subthreshold oscillations were observed at membrane potentials below AP threshold (*bottom*, −48 mV), between APs at membrane potentials above AP threshold (*middle*, −43 mV), and after inactivation of sodium channels underlying APs (*top*, −40 mV). The dotted boxes include 1 s of recordings (*top records*) that are also shown at higher resolution (*bottom records*), revealing gamma frequency oscillations at −48 mV (*bottom*, red), −43 mV (*middle*, green), and −40 mV (*top*, blue). *B*: a power spectrum of the oscillations confirmed that some of the subthreshold oscillations at −48 mV (red), −43 mV (green), and −40 mV (blue) were in the alpha and gamma frequency ranges but no higher. *C*: low concentration of tetrodotoxin (TTX, 0.01 µM, *top*) blocked sodium channels responsible for AP generation, but subthreshold oscillations were still observed, which were then blocked by high concentration of TTX (10 µM, *bottom*). The dotted boxes include 1 s of recordings (*top records*) that are also shown at higher resolution (*bottom records*) during 0.01 µM TTX (*top*, orange) and 10 µM TTX (*bottom*, brown). *D*: addition of QX-314 (5 mM) to the intracellular solution also blocked the subthreshold oscillations (dotted black boxes). *E*: power spectra of the recordings shown in *C* (*left*) and *D* (*right*). Before TTX (green), peaks were observed in the power spectrum, which were partially blocked by 0.01 µM TTX (orange) and almost completely blocked by 10 µM TTX (brown). QX-314 (5 mM; black) also blocked the subthreshold oscillations.

gamma ranges. The effects quickly returned to baseline levels following washout with aCSF. KA application ($n = 4$) also increased the activity of the SubCD neuronal population, as evident in the recordings (Fig. 4*D*) and power spectrum (Fig. 4*E*). KA induced significant peaks of activation in the alpha and low gamma range [$F = 6.11$ (2, 6), $P < 0.05$], with peaks at 15 Hz ($P < 0.01$) and 30 Hz ($P < 0.001$). A graph of ERSPs was generated using 9 min of recordings taken during a 10-min KA exposure and 5 min following exposure (Fig. 4*F*). The effect of KA began at *minute 2*, gradually increasing activity with a peak effect after 4 min, when specific peaks of activity in the alpha and low gamma range were manifested. Unlike NMDA, the effects of KA persisted after the end application (see *minutes 9–13* in Fig. 4*F*).

The effect of cholinergic input on the population of neurons in the SubCD was tested using CAR ($n = 4$, Fig. 4*G*). The power spectrum revealed statistically significant peaks of activity in the alpha (low levels), low gamma, and mid gamma range (Fig. 4*H*) [$F = 15.94$ (2, 6), $P < 0.01$], with peaks at 10 Hz ($P < 0.05$), 30 Hz ($P < 0.001$), and 45 Hz ($P < 0.001$). A graph of ERSPs was generated using 10 min of recordings during CAR exposure (Fig. 4*I*). The effect of CAR started at *minute 3*, with a peak effect after 5 min. During the peak effect, CAR induced activity at specific frequencies in the alpha, low gamma, and medium gamma ranges. Like KA, the effect of CAR persisted following washout. The population of neurons in the SubCD appears to generate gamma frequency activity in response to excitatory glutamatergic and cholinergic inputs.

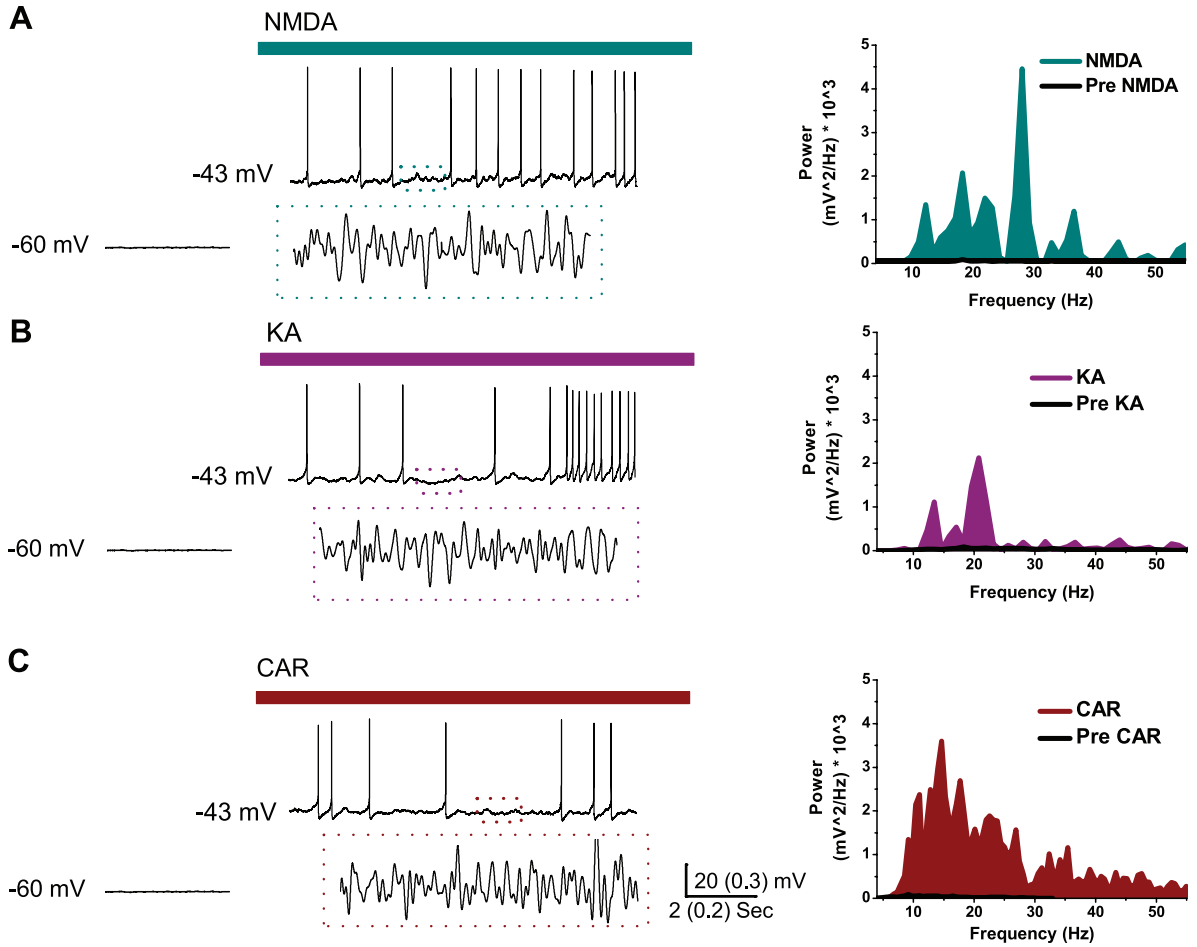

Fig. 3. Gamma frequency subthreshold oscillations in SubCD neurons induced by cholinergic and glutamatergic inputs. *A*: recording of a SubCD neuron before application of 4 μM *N*-methyl-D-aspartic acid (NMDA; −60 mV), and during the peak response to NMDA (−43 mV). The green dotted boxes include 1-s recordings (*top record*, higher resolution below) revealing gamma frequency oscillations during superfusion of NMDA. The power spectrum (*right*) of the subthreshold oscillations revealed peaks at alpha and gamma band, with a high amplitude peak at 28 Hz during NMDA exposure (green), compared with control (black). *B*: kainic acid (KA; 1 μM) also depolarized the membrane to −43 mV and subthreshold oscillations were observed. The purple dotted boxes include 1-s recordings (*top record*, higher resolution below), revealing gamma frequency oscillations during the response to KA. The power spectrum (*right*) of the subthreshold oscillations revealed peaks at 14 Hz and 21 Hz during KA exposure (purple) compared with control (black). *C*: subthreshold oscillations were observed after superfusion with CAR (30 μM). The red dotted boxes include a 1-s recording (*top record*, higher resolution below), revealing alpha and gamma frequency oscillations during CAR exposure. The power spectrum (*right*) of the subthreshold oscillations following CAR (red) showed peaks at 15, 23 and 34 Hz, compared with control (black).

DISCUSSION

In the present study, we found that the SubCD was able to manifest gamma band activity during both single cell and population response recordings. Two cell types were identified, which were distinguished by their high versus low initial AP-firing properties. Gamma frequency subthreshold oscillations were found to underlie the gamma frequency firing of these neurons. The subthreshold oscillations were blocked by the sodium channel blockers TTX extracellularly applied and QX-314 in the recording pipette, indicating a sodium-dependent mechanism. Subthreshold oscillations were also observed following depolarization of SubCD neurons using NMDA, KA, and CAR, at both single cell (whole cell patch clamp) and nuclear levels (population responses). Thus gamma band oscillatory activity is a phenomenon observed in single neurons and the population of neurons in the SubCD.

Single cell recordings. Our results show that the initial AP frequency of some SubCD neurons was greater than gamma frequency, but the AP frequency of all SubCD neurons plateaued in the gamma range (20–80 Hz). In vivo extracellular recordings from "PGO-on" neurons revealed high-frequency spike bursts (>500 Hz) and tonic firing at 25–100 Hz (9), suggesting that the cells that initially displayed high-frequency APs may be putative "PGO-on" cells in the rat. In the prefrontal cortex, striatum, and subthalamic nucleus, a linear increase in AP frequency was observed with no plateau (1, 4). On the other hand, pyramidal cells in mouse neocortex plateaued below gamma frequency (45). In the PPN, all neurons plateaued at gamma frequency and had gamma frequency membrane oscillations (34) due to the presence of P/Q-type calcium channels (22).

All SubCD neurons exhibited subthreshold oscillations in the gamma range (Fig. 2). These gamma band oscillations appeared in conjunction with other frequencies, such as alpha, but it is likely that the gamma frequencies would contribute to REM sleep generation. Gamma frequency subthreshold oscil-

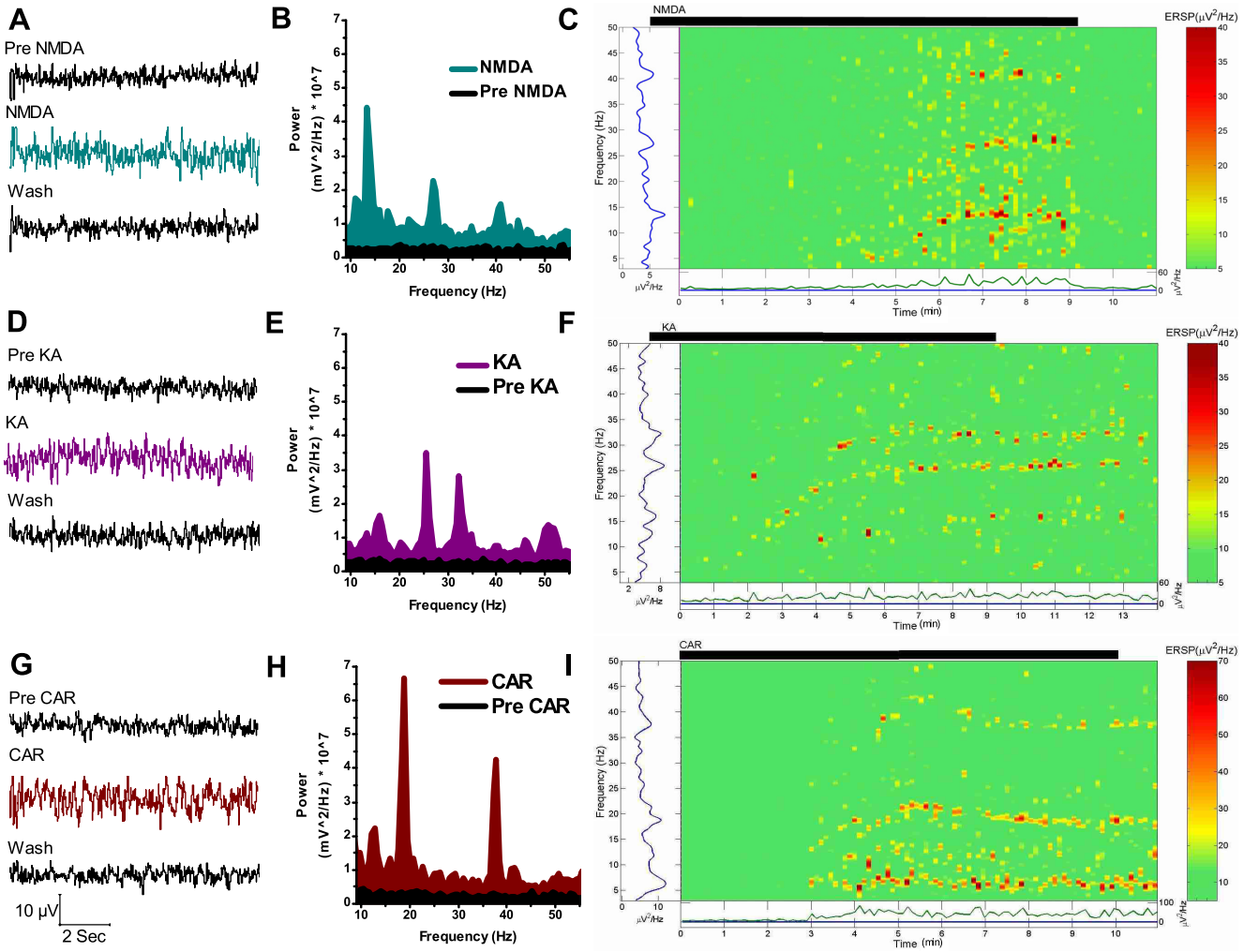

Fig. 4. Population response recordings revealed gamma frequency activity. *A*: one second records before (*top*, black), during (*middle*, green), and after washout (*bottom*, black) of NMDA (10 μM). *B*: power spectrum of the 20-s recordings, including the 1-s shown in *A*, revealed an overall increase in activity as well as specific peaks in the alpha and gamma ranges during NMDA exposure (green) compared with control (black). *C*: a graph of ERSPs was generated using 9 min of recordings during NMDA exposure and 2 min washout. NMDA took effect at *minute 3*, and the peak effect was observed between *minutes 5* and *9*. *D*: 1-s sample records before (*top*, black), during (*middle*, purple), and after washout (*bottom*, black) of KA (2 μM). *E*: power spectrum of 20-s recordings, including the 1 s shown in *D*, revealed specific peaks in the alpha and gamma ranges during KA exposure (purple) compared with control (black). *F*: graph of event-related spectral perturbations (ERSPs) was generated using 9 min of recordings taken during a 10-min KA exposure and 5 min after exposure. The effect of KA began at *minute 2*, gradually increasing activity with a peak effect after 4 min. *G*: 1-s sample records before (*top*, black), during (*middle*, red), and after washout (*bottom*, black) of CAR (50 μM). *H*: power spectrum of 20-s recordings, including the 1 s shown in *G*, revealed peaks of activity in the alpha, low gamma, and mid gamma range during CAR exposure (red) compared with control (black). *I*: graph of ERSPs was generated using 10 min of recordings during CAR exposure. The effect of CAR started at *minute 3*, with a peak effect after 5 min.

lations may underlie gamma frequency APs in these neurons, and, at higher membrane potentials, the neurons would be more likely to fire at the peak of the oscillation. We did not observe any differences in oscillation frequency between the two cell types described in Fig. 1, which may be expected, considering the difference between the two cell types was only observed during the initiation of the current steps.

The subthreshold oscillations were blocked by TTX and QX-314, indicating a sodium-dependent mechanism. Low concentration (0.01 μM) of TTX was sufficient to block AP generation, but high concentration (10 μM) was required to completely block subthreshold oscillations. A similar phenomenon has been described in the cortex, where APs and subthreshold oscillations were observed before bath application of TTX, APs were blocked after a 30-s application of 10 μM TTX, and voltage-gated persistent sodium channels mediating the subthreshold oscillations were blocked only after 90 s (23). Two populations of sodium channels, TTX-resistant and TTX-sensitive, have also been described in the dorsal root ganglia (16, 32) and entorhinal cortex (42). The SubCD may contain two populations of sodium channels: a TTX-sensitive subtype that mediates AP generation and is blocked by nanomolar concentrations of TTX, and a TTX-resistant subtype that mediates subthreshold oscillations and is only blocked by micromolar concentrations of TTX.

Subthreshold oscillations were also observed during exposure of NMDA, KA, or CAR. In physiological conditions, glutamatergic and cholinergic inputs may provide the necessary activation to induce these subthreshold currents to reach threshold and promote gamma band frequency APs. It is

interesting to note that, even though all three neuroactive agents depolarized the recorded neurons to approximately the same levels, unique patterns of activity were observed following each agent (Fig. 3). For example, NMDA produced a high amplitude peak at 28 Hz, whereas KA exposure produced a high amplitude peak at 21 Hz in the power spectrum, even though both depolarized the cell to −43 mV. It is clear that neurotransmitter actions can initiate a dynamic range of gamma frequency subthreshold oscillations.

Population response recordings. Population recordings represent the sum of the activity of the neurons near the recording site. Our population response studies revealed that the population of neurons in the SubCD is capable of generating specific frequencies of activity when pharmacologically stimulated with CAR, NMDA, or KA. NMDA had a longer latency to effect than did CAR or KA, and its effects quickly waned following washout. On the other hand, the effects of CAR and KA persisted beyond the end of drug application and during washout. After application of KA, specific frequencies in the gamma range were observed. It has been hypothesized that activation of the KA receptor in the PPN is important for REM sleep (8), and KA injections into the SubCD produced a REM sleep-like state (5). Perhaps activation of efferent targets of the SubCD at these frequencies is important for REM sleep generation.

Single cell and population responses to NMDA and CAR were similar; both increased activity at frequencies in the low to mid gamma range. However, differences were observed between our single cell and population studies following KA exposure; activity in the low gamma range was observed in single cells, but mid gamma activity was observed in population response recordings. Perhaps the lower concentration of KA used in single cell studies was not sufficient to drive gamma band activity, but the higher concentration used in population studies shifted activity to higher frequencies.

Limitations. A number of essential experiments were beyond the scope of the present studies. The SubCD contains a number of glutamatergic and electrically coupled GABAergic neurons (6, 10, 18), and we have not yet determined the neurotransmitter phenotypes of the high versus low firing frequency neurons. Moreover, the amplitudes of the subthreshold oscillations were not measured at different membrane potentials due to their variability, but it appears that the oscillations increased in amplitude at more depolarized membrane potentials (Fig. 2).

We determined that the depolarizing phase of the subthreshold oscillations was a sodium current, but we did not identify the location of the sodium channels, which could be located on the dendrites or the soma of the neurons. Furthermore, we have not yet identified the ionic currents responsible for the downward phase of the oscillation, which is likely a potassium current, as observed in the cortex (23).

Metabotropic glutamate receptors generate slow postsynaptic responses and contribute to a delayed neuronal response (40). We did not test the effects of metabotropic glutamate receptor agonists on gamma band activity; perhaps gamma band activity is initiated by ionotropic glutamate receptors and is maintained by the prolonged activity of metabotropic glutamate receptors. These data would reveal further details of the mechanisms behind SubCD gamma band activity.

Physiological significance. Potent activation of SubCD neurons appears to lead to two signals, one beginning at high frequency and then settling at gamma band and the second monotonically generating gamma band activation. This suggests that the two cell types may code for different initial effects at their targets. The significance of the plateau levels at gamma band frequency suggests that, as long as SubCD activation is maintained, its targets receive continuous gamma band activation. This may result in generating gamma band activity in these targets.

The differential effects of CAR, NMDA, and KA suggest that the population as a whole may be modulated by both cholinergic and glutamatergic inputs to manifest activity at different frequencies. One potential control schema is suggested by the effects of these agents in population response recordings (Fig. 4). NMDA increased activity at almost all frequencies, with peaks at 15, 27, and 40 Hz, while CAR increased activity at 20 and 37 Hz, and KA increased activity at 15, 25, and 33 Hz. NMDA and KA together may preferentially induce activity at low gamma, while CAR and NMDA together may preferentially induce activity at mid and high gamma frequencies. This suggests that the combined influence of two transmitters may modulate separate frequencies of activity.

Because gamma waves can occur during slow wave states and anesthesia, a close relation to consciousness has been questioned (37). It was suggested that consciousness is associated with continuous gamma band activity, as opposed to an interrupted pattern of activity (37). This raises the question of how a circuit can maintain such rapid, recurrent activation. Expecting a circuit of 5 or 10 synapses to reliably relay 40 Hz cycling without failing is unrealistic. Without the intrinsic properties afforded by rapidly oscillating channels, such as those described here for SubCD, gamma band activity could not be maintained. The combination of channels capable of fast oscillations and circuitry that involves activating these channels is required for the maintenance of gamma band activity.

These results suggest that a similar mechanism for achieving temporal coherence in the cortex is also present in the SubCD. Rather than participating in the temporal binding of sensory events (39), gamma band activity manifested in the SubCD may help stabilize coherence related to REM sleep. This provides a stable activation state during paradoxical sleep and relays such activation to the thalamus, which may participate in cortical activation via P waves, and/or the hippocampus. Much work is needed to support this speculation, but the intriguing findings described here certainly provide a starting point for such investigations.

GRANTS

This work was supported by National Institutes of Health award R01 NS020246, by core facilities of the Center for Translational Neuroscience supported by P20 RR020146, and FONCYT Agencia Nacional de Promoción Científica y Tecnológica, BID 1728 OC.AR.PICT 2007-01009, PICT 2008-2019, and PIDRI-PRH 2007 (to Dr. Urbano).

DISCLOSURES

No conflicts of interest, financial or otherwise, are declared by the author(s).

REFERENCES

1. **Azouz R, Gray CM, Nowak LG, McCormick DA.** Physiological properties of inhibitory interneurons in cat striate cortex. *Cereb Cortex* 7: 534–545, 1997.

2. **Baghdoyan HA, Rodrigo-Angulo ML, McCarley RW, Hobson JA.** A neuroanatomical gradient in the pontine tegmentum for the cholinoceptive induction of desynchronized sleep signs. *Brain Res* 414: 245–261, 1987.
3. **Baghdoyan HA, Rodrigo-Angulo ML, McCarley RW, Hobson JA.** Site-specific enhancement and suppression of desynchronized sleep signs following cholinergic stimulation of three brainstem regions. *Brain Res* 306: 39–52, 1984.
4. **Barraza D, Kita H, Wilson CJ.** Slow spike frequency adaptation in neurons of the rat subthalamic nucleus. *J Neurophysiol* 102: 3689–3697, 2009.
5. **Boissard R, Gervasoni D, Schmidt MH, Barbagli B, Fort P, Luppi PH.** The rat ponto-medullary network responsible for paradoxical sleep onset and maintenance: a combined microinjection and functional neuroanatomical study. *Eur J Neurosci* 16: 1959–1973, 2002.
6. **Brown RE, Winston S, Basheer R, Thakkar MM, McCarley RW.** Electrophysiological characterization of neurons in the dorsolateral pontine rapid-eye-movement sleep induction zone of the rat: Intrinsic membrane properties and responses to carbachol and orexins. *Neuroscience* 143: 739–755, 2006.
7. **Datta S.** Activation of phasic pontine-wave generator: a mechanism for sleep-dependent memory processing. *Sleep Biological Rhythms* 4: 16–26, 2006.
8. **Datta S.** Evidence that REM sleep is controlled by the activation of brain stem pedunculopontine tegmental kainate receptor. *J Neurophysiol* 87: 1790–1798, 2002.
9. **Datta S, Hobson JA.** Neuronal activity in the caudolateral peribrachial pons: relationship to PGO waves and rapid eye movements. *J Neurophysiol* 71: 95–109, 1994.
10. **Datta S, Maclean RR.** Neurobiological mechanisms for the regulation of mammalian sleep-wake behavior: reinterpretation of historical evidence and inclusion of contemporary cellular and molecular evidence. *Neurosci Biobehav Rev* 31: 775–824, 2007.
11. **Datta S, Patterson EH, Siwek DF.** Brainstem afferents of the cholinoceptive pontine wave generation sites in the rat. *Sleep Res Online* 2: 79–82, 1999.
12. **Datta S, Siwek DF, Patterson EH, Cipolloni PB.** Localization of pontine PGO wave generation sites and their anatomical projections in the rat. *Synapse* 30: 409–423, 1998.
13. **Datta S, Siwek DF, Stack EC.** Identification of cholinergic and noncholinergic neurons in the pons expressing phosphorylated cyclic adenosine monophosphate response element-binding protein as a function of rapid eye movement sleep. *Neuroscience* 163: 397–414, 2009.
14. **Delorme A, Makeig S.** EEGLAB: an open source toolbox for analysis of single-trial EEG dynamics including independent component analysis. *J Neurosci Methods* 134: 9–21, 2004.
15. **Eckhorn R, Bauer R, Jordan W, Brosch M, Kruse W, Munk M, Reitboeck HJ.** Coherent oscillations: a mechanism of feature linking in the visual cortex? Multiple electrode and correlation analyses in the cat. *Biol Cybern* 60: 121–130, 1988.
16. **Elliott AA, Elliott JR.** Characterization of TTX-sensitive and TTX-resistant sodium currents in small cells from adult rat dorsal root ganglia. *J Physiol* 463: 39–56, 1993.
17. **Gray CM, Singer W.** Stimulus-specific neuronal oscillations in orientation columns of cat visual cortex. *Proc Natl Acad Sci USA* 86: 1698–1702, 1989.
18. **Heister DS, Hayar A, Charlesworth A, Yates C, Zhou YH, Garcia-Rill E.** Evidence for electrical coupling in the subcoeruleus (SubC) nucleus. *J Neurophysiol* 97: 3142–3147, 2007.
19. **Heister DS, Hayar A, Garcia-Rill E.** Cholinergic modulation of GABAergic and glutamatergic transmission in the dorsal subcoeruleus: mechanisms for REM sleep control. *Sleep* 32: 1135–1147, 2009.
20. **Jouvet-Mounier D, Astic L.** Study of the course of sleep in the young rat during the 1st postnatal month. *CR Seances Soc Biol Fil* 162: 119–123, 1968.
21. **Karlsson KA, Gall AJ, Mohns EJ, Seelke AM, Blumberg MS.** The neural substrates of infant sleep in rats. *PLoS Biol* 3: e143, 2005.
22. **Kezunovic N, Urbano FJ, Simon C, Hyde J, Smith K, Garcia-Rill E.** Mechanism behind gamma band activity in the pedunculopontine nucleus (PPN). *Eur J Neurosci*. In press.
23. **Llinas RR, Grace AA, Yarom Y.** In vitro neurons in mammalian cortical layer 4 exhibit intrinsic oscillatory activity in the 10- to 50-Hz frequency range. *Proc Natl Acad Sci USA* 88: 897–901, 1991.
24. **Lu J, Sherman D, Devor M, Saper CB.** A putative flip-flop switch for control of REM sleep. *Nature* 441: 589–594, 2006.
25. **Marks GA, Farber J, Roffwarg HP.** Metencephalic localization of ponto-geniculo-occipital waves in the albino rat. *Exp Neurol* 69: 667–677, 1980.
26. **Mavanji V, Ulloor J, Saha S, Datta S.** Neurotoxic lesions of phasic pontine-wave generator cells impair retention of 2-way active avoidance memory. *Sleep* 27: 1282–1292, 2004.
27. **Middleton SJ, Racca C, Cunningham MO, Traub RD, Monyer H, Knopfel T, Schofield IS, Jenkins A, Whittington MA.** High-frequency network oscillations in cerebellar cortex. *Neuron* 58: 763–774, 2008.
28. **Mitler MM, Dement WC.** Cataplectic-like behavior in cats after microinjections of carbachol in pontine reticular formation. *Brain Res* 68: 335–343, 1974.
29. **Mouret J, Delorme F, Jouvet M.** [Lesions of the pontine tegmentum and sleep in rats]. *C R Seances Soc Biol Fil* 161: 1603–1606, 1967.
30. **Palva S, Monto S, Palva JM.** Graph properties of synchronized cortical networks during visual working memory maintenance. *Neuroimage* 49: 3257–3268, 2010.
31. **Phillips S, Takeda Y.** Greater frontal-parietal synchrony at low gamma-band frequencies for inefficient than efficient visual search in human EEG. *Int J Psychophysiol* 73: 350–354, 2009.
32. **Roy ML, Narahashi T.** Differential properties of tetrodotoxin-sensitive and tetrodotoxin-resistant sodium channels in rat dorsal root ganglion neurons. *J Neurosci* 12: 2014–2111, 1992.
33. **Sanford LD, Morrison AR, Mann GL, Harris JS, Yoo L, Ross RJ.** Sleep patterning and behaviour in cats with pontine lesions creating REM without atonia. *J Sleep Res* 3: 233–240, 1994.
34. **Simon C, Kezunovic N, Ye M, Hyde J, Hayar A, Williams DK, Garcia-Rill E.** Gamma band unit activity and population responses in the pedunculopontine nucleus. *J Neurophysiol* 104: 463–474, 2010.
35. **Singer W.** Synchronization of cortical activity and its putative role in information processing and learning. *Annu Rev Physiol* 55: 349–374, 1993.
36. **Takakusaki K, Kitai ST.** Ionic mechanisms involved in the spontaneous firing of tegmental pedunculopontine nucleus neurons of the rat. *Neuroscience* 78: 771–794, 1997.
37. **Vanderwolf CH.** What is the significance of gamma wave activity in the pyriform cortex? *Brain Res* 877: 125–133, 2000.
38. **Vanni-Mercier G, Sakai K, Lin JS, Jouvet M.** Mapping of cholinoceptive brainstem structures responsible for the generation of paradoxical sleep in the cat. *Arch Ital Biol* 127: 133–164, 1989.
39. **Velik R.** From single neuron-firing to consciousness–towards the true solution of the binding problem. *Neurosci Biobehav Rev* 34: 993–1001, 2010.
40. **Von Bohlen und Halbach O, Dermietzel R (Editors).** *Neurotransmitters and Neuromodulators*. Weinheim, Germany: Wiley-VCH, 2006.
41. **Voss U, Holzmann R, Tuin I, Hobson JA.** Lucid dreaming: a state of consciousness with features of both waking and non-lucid dreaming. *Sleep* 32: 1191–1200, 2009.
42. **White JA, Alonso A, Kay AR.** A heart-like Na+ current in the medial entorhinal cortex. *Neuron* 11: 1037–1047, 1993.
43. **Whittington MA, Stanford IM, Colling SB, Jefferys JG, Traub RD.** Spatiotemporal patterns of gamma frequency oscillations tetanically induced in the rat hippocampal slice. *J Physiol* 502: 591–607, 1997.
44. **Yamamoto K, Mamelak AN, Quattrochi JJ, Hobson JA.** A cholinoceptive desynchronized sleep induction zone in the anterodorsal pontine tegmentum: spontaneous and drug-induced neuronal activity. *Neuroscience* 39: 295–304, 1990.
45. **Zhou L, Gall D, Qu Y, Prigogine C, Cheron G, Tissir F, Schiffmann SN, Goffinet A.** Maturation of "neocortex isole" in vivo in mice. *J Neurosci* 30: 7928–7939, 2010.